Journal of Biomolecular NMR, **15:** 115–124, 1999.
KLUWER/ESCOM

Backbone dynamics of the human CC-chemokine eotaxin

Jiqing Ye, Kristen L. Mayer & Martin J. Stone*
Department of Chemistry, Indiana University, Bloomington, IN 47405-0001, U.S.A.

Received 18 May 1999; Accepted 5 August 1999

Key words: chemokines, disulfide bond isomerization, eotaxin, NMR relaxation, protein backbone dynamics

Abstract

Eotaxin is a CC chemokine with potent chemoattractant activity towards eosinophils. ^{15}N NMR relaxation data have been used to characterize the backbone dynamics of recombinant human eotaxin. ^{15}N longitudinal (R_1) and transverse (R_2) auto relaxation rates, heteronuclear {^{1}H}-^{15}N steady-state NOEs, and transverse cross-relaxation rates (η_{xy}) were obtained at 30 °C for all resolved backbone secondary amide groups using ^{1}H-detected two-dimensional NMR experiments. Ratios of transverse auto and cross relaxation rates were used to identify NH groups influenced by slow conformational rearrangement. Relaxation data were fit to the extended model free dynamics formalism, yielding parameters describing axially symmetric molecular rotational diffusion and the internal dynamics of each NH group. The molecular rotational correlation time (τ_m) is 5.09 ± 0.02 ns, indicating that eotaxin exists predominantly as a monomer under the conditions of the NMR study. The ratio of diffusion rates about unique and perpendicular axes ($D_\parallel/D_\perp$) is 0.81 ± 0.02. Residues with large amplitudes of subnanosecond motion are clustered in the N-terminal region (residues 1–19), the C-terminus (residues 68–73) and the loop connecting the first two β-strands (residues 30–37). N-terminal flexibility appears to be conserved throughout the chemokine family and may have implications for the mechanism of chemokine receptor activation. Residues exhibiting significant dynamics on the microsecond–millisecond time scale are located close to the two conserved disulfide bonds, suggesting that these motions may be coupled to disulfide bond isomerization.

Abbreviations: 2D, 3D, two-, three-dimensional; HSQC, heteronuclear single-quantum coherence; MCP-1, monocyte chemoattractant protein-1; NOE, nuclear Overhauser effect; RANTES, regulated upon activation normal T-cell expressed and secreted; rmsd, root-mean-square deviation; vMIP-II, viral macrophage inflammatory protein-II.

Introduction

Chemokines are a superfamily of small secreted proteins whose primary function is to attract leukocytes to the sites of inflammation (Baggiolini et al., 1997; Luster, 1998). This activity is central to the inflammatory response against infection as well as to many inflammatory diseases. Therefore, inhibition of chemokine activity may be an effective therapeutic strategy against inflammatory disease. Most chemokines can be classified into two well-characterized subfamilies designated CXC (or α) and CC (or β), according to whether the first two of four conserved cysteine residues are separated by a single amino acid or adjacent, respectively. Recently, novel chemokines have been discovered whose sequences suggest the existence of two additional subfamilies designated C (Kelner et al., 1994) and CX_3C (Bazan et al., 1997).

Chemokine receptors are seven transmembrane helix G-protein coupled receptors (Murphy, 1994; Luster, 1998). Little is known about the details of their

*To whom correspondence should be addressed. E-mail: mastone@indiana.edu

The supplementary material includes one figure, summarizing the NMR data for the secondary structure determination of eotaxin, and three tables, listing: (1) the relaxation parameters (R_1, R_2, NOE, and η_{xy}); (2) the model-free dynamics parameters (S_s^2, S_f^2, τ_e and R_{ex}) calculated for the axially symmetric molecular rotational diffusion model; and (3) the model-free parameters calculated for the isotropic diffusion model. The relaxation data have been deposited with the BMRB (accession no. 4390).

structures or the molecular mechanism of receptor activation by chemokines. It has been proposed, based on mutagenesis data, that the ligand–receptor interaction occurs via a two-step mechanism in which the N-loop of the chemokine (between the second cysteine and the first β-strand) initially binds to the inactive state of the receptor, then the N-terminus of the chemokine (preceding the first cysteine) makes a second receptor contact, causing the receptor to undergo a conformational change to its activated state (Murphy, 1994; Crump et al., 1997, 1998). The second step of this mechanism may require that the chemokine itself has some conformational flexibility. Thus, both the structure and dynamics of chemokines are of interest in understanding the mechanism of receptor activation.

Eotaxin is a CC-chemokine with specific chemoattractant activity for eosinophils and basophils, mediated through the receptor CCR3. Eotaxin appears to be a pivotal chemokine involved in eosinophil accumulation in vivo and is likely the most relevant chemokine to eosinophilia-related diseases such as allergic reactions (e.g. asthma) and parasitic infestations (Weller, 1994; Rothenberg et al., 1995; Baggiolini, 1996; Garcia-Zepeda et al., 1997; Luster, 1998). The specificity of eotaxin for the receptor CCR3 and its predominant role in these diseases make it a favored target for drug design. The three-dimensional (3D) structure of eotaxin has been determined recently based on homonuclear and ^{15}N-edited NMR data (Crump et al., 1998). The structure is similar to those of other chemokines and consists of an unstructured N-terminal region, a three-stranded antiparallel β-sheet, and a C-terminal overlying α-helix. The β_1- and β_2-strands are connected by a relatively long loop whereas the β_2- and β_3-strands and the β_3-strand and α-helix are connected by short turns. The two conserved disulfide bonds link the N-terminal region to the β_1-β_2 loop and the β_3-strand. In this paper we present the backbone dynamics of eotaxin determined by analysis of ^{15}N NMR relaxation parameters.

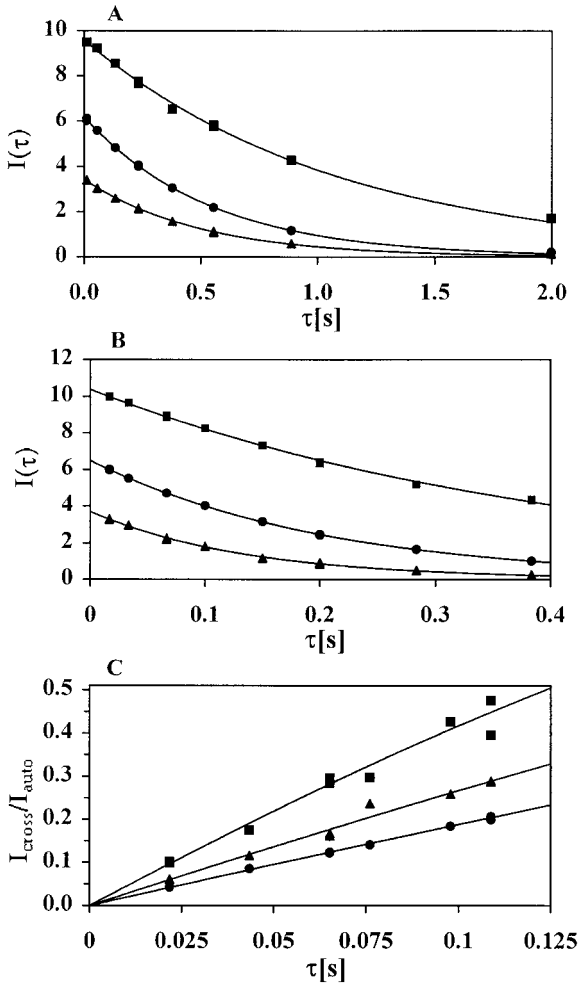

Figure 1. Examples of (A) R_1, (B) R_2 and (C) η_{xy} curve fits. In (A) and (B), the peak intensity I(τ) is plotted as a function of time for K68 (●), L13 (▲), and S4 (■). The peak intensities are shown on an arbitrary absolute scale. The uncertainties in the peak intensities are less than 0.1 unit for R_1 and less than 0.05 unit for R_2. K68 (●) is one of the best fits, L13 (▲) is about average, and S4 (■) is among the worst. In (C), the ratio of intensities in cross-relaxation and auto-relaxation experiments (I_{cross}/I_{auto}; Kroenke et al., 1998) is plotted as a function of time for S69 (●), R16 (▲), and A51 (■).

Materials and methods

Uniformly ^{15}N-labeled or ^{13}C,^{15}N-doubly labeled eotaxin was prepared as an N-terminally $(His)_6$-tagged fusion protein by expression in *Escherichia coli*. The fusion protein was purified by Ni^{2+}-affinity chromatography, the fusion leader was removed proteolytically, and the mature protein (with a native N-terminus) was further purified by cation exchange chromatography. N-terminal sequencing, amino acid composition analysis, and mass spectrometry confirmed that the primary structure of the recombinant eotaxin was as expected for native eotaxin (Kitaura et al., 1996; Garcia-Zepeda et al., 1997).

Protein samples for NMR analysis were dissolved at a concentration of ~0.8–1.0 mM in 20 mM deuterated sodium acetate, 0.02% NaN_3, 10% D_2O, pH 5.0. All NMR measurements were performed at 30 °C on a Varian Unity INOVA 500 MHz spectrometer.

Backbone and C_β/H_β resonance assignments were achieved using standard heteronuclear and triple resonance methods. The secondary structure deduced from short- and medium-range NOEs, $^3J_{HNH\alpha}$ coupling constants, and secondary chemical shifts is consistent with the structure of Crump et al. (1998); these data are summarized in the Supplementary material.

^{15}N longitudinal (R_1) and transverse (R_2) relaxation rates, heteronuclear $\{^1H\}$-^{15}N NOEs, and transverse cross-relaxation rates (η_{xy}) were measured using 2D ^1H-^{15}N correlation pulse sequences (Farrow et al., 1994; Kroenke et al., 1998). η_{xy} is the rate constant for cross-relaxation between in-phase magnetization (S_x or S_y) and antiphase magnetization ($2I_zS_x$ or $2I_zS_y$, respectively). This cross-relaxation process results from cross-correlation or interference between chemical shift anisotropy and dipolar relaxation mechanisms (Tjandra et al., 1996; Kroenke et al., 1998). Delay values used were: $\tau = 11^*$, 56, 133, 233^*, 377, 555^*, 888, and 1998^* ms for the R_1 experiment; $\tau = 17^*$, 33, 67^*, 100, 150, 200^*, 284, and 384^* ms for the R_2 experiment; and $\tau = 22^*$, 43, 65^*, 76, 98, and 109^* ms for the η_{xy} experiment; asterisks indicate time points duplicated to allow estimation of uncertainties. Two identical pairs of $\{^1H\}$-^{15}N NOE experiments were recorded. In one experiment of each pair, protons were saturated for 3 s following the 5 s recycle delay by application of 120° pulses (field strength 10 kHz), spaced 5 ms apart. In the other experiment, a 12 s recycle delay was used without proton saturation.

Relaxation rate constants were obtained by weighted fits of the peak heights in the 2D spectra as described previously (Stone et al., 1993; Kroenke et al., 1998). Peak height uncertainties were determined from the duplicate time points as described (Stone et al., 1993) and uncertainties in relaxation rate constants were taken to be the standard errors of the fitted parameters. Steady-state NOEs were calculated as the ratios of the cross peak heights in the presence and the absence of proton saturation. The NOE for each NH group was calculated separately from each of the two repeated pairs of experiments. The NOE was taken to be the average of the two measurements. The standard deviation of the differences between the two measurements was divided by $\sqrt{2}$ to yield the absolute uncertainty in the NOE (assumed to be the same for all peaks).

The relaxation parameters were fitted to the Lipari–Szabo model free dynamics formalism (Lipari and Szabo, 1982a, b) or extended versions thereof (Clore et al., 1990a, b; Barbato et al., 1992) using the program Modelfree 4.0 (Palmer et al., 1991; Mandel et al., 1995). Initially, the components of the molecular rotational diffusion tensor were estimated from the R_2/R_1 ratios of 36 residues (Kay et al., 1989; Clore et al., 1990b; Barbato et al., 1992) using the program r2r1_diffusion, for the cases of isotropic and axially symmetric diffusion tensors, and the program quadric_diffusion for the case of a fully anisotropic diffusion tensor; these programs were provided by Dr. A.G. Palmer, III (Columbia University). Isotropic molecular rotational diffusion was characterized by a single correlation time τ_m. Axially symmetric diffusion was defined by the ratio of diffusion rates about unique and perpendicular axes ($D_\parallel/D_\perp$), a correlation time τ_m [defined as $(2D_\parallel + 4D_\perp)^{-1}$], and the orientation of the unique axis relative to the coordinates of the average energy minimized NMR structure [PDB code 1EOT; Crump et al., 1998] (Tjandra et al., 1995). Fully anisotropic diffusion was defined by the diffusion rates about three orthogonal axes (D_{xx}, D_{yy}, and D_{zz}) and the orientation of the axis system relative to the NMR structure (Tjandra et al., 1995). R_2/R_1 data for 14 residues (A3, S4, V5, T7, T8, C9, R16, K33, A38, L45, K68, S69, T71, K73) were excluded from the initial estimation of diffusion tensor components on the basis that the corresponding NH groups have large amplitudes of fast time scale internal motions (NOE < 0.5). Of the remaining 43 residues, an additional 7 residues (N12, L13, T30, S31, Q36, K37, A51) were then excluded on the basis that the R_2/η_{xy} values for these residues exceed the average R_2/η_{xy} value (1.80) by more than one standard deviation (0.47), indicating that R_2 values for these residues are influenced by slow conformational exchange (Fushman and Cowburn, 1998). After selection of the appropriate model to describe the molecular rotational diffusion, the data for each NH group were then fitted to each of the following five internal motional models (Mandel et al., 1995, 1996). Model 1 yields only an order parameter (S_f^2) representing the amplitude of fast (<20 ps) internal motions (Lipari and Szabo, 1982a, b). Model 2 yields an order parameter (S_f^2) and an effective internal correlation time (τ_f) for fast (<500 ps) internal motions (Lipari and Szabo, 1982a, b). Model 3 yields an order parameter (S_f^2) for internal motions faster than ~20 ps and an R_{ex} term representing the contribution of μs–ms time scale motions to the transverse relaxation rate constant R_2 (Kay et al., 1989; Palmer et al., 1996). Model 4 yields an order parameter (S_f^2) and internal correlation time (τ_f) for motions faster than 500 ps and also an R_{ex} term. Finally, model 5 yields an

order parameter (S_f^2) for internal motions faster than ~20 ps and an order parameter (S_s^2) and corresponding correlation time (τ_s) for internal motions slower than 500 ps but faster than τ_m (Clore et al., 1990a, b). The difference between parallel and perpendicular components of the ^{15}N chemical shift tensor ($\sigma_\parallel - \sigma_\perp$) was taken to be −170 ppm. Fitting procedures and model selection criteria have been described previously by Mandel et al. (1995). Upon selection of the optimum model for each residue, a final optimization was performed in which the molecular diffusion parameters and the selected internal dynamics parameters for each NH group were optimized simultaneously. Uncertainties in the dynamics parameters were determined using Monte Carlo simulations carried out by the Modelfree program (Stone et al., 1993). Data presented here are for an axially symmetric molecular diffusion model; data for both axially symmetric and isotropic diffusion models are listed in the Supplementary material.

Results

Relaxation parameters

Relaxation data were obtained for 57 of the 65 backbone secondary amide nitrogen nuclei in eotaxin. The eight NH groups not included were two that did not appear in the HSQC spectrum (C10 and F11), two pairs of overlapped NH peaks (N15/K44 and D48/I29) and one pair (C34 and Q67) that was too poorly resolved to allow accurate measurement of peak heights. Peak intensities observed in the R_1, R_2 and η_{xy} experiments fit well to the expected relaxation equations. Examples are illustrated in Figure 1.

The R_1, R_2, R_2/R_1 and NOE values for each residue are shown in Figure 2A–D. R_1, R_2 and NOE values are all significantly lower than average in the N- and C-terminal regions of the protein, indicating the presence of considerable motion on a fast (picosecond–nanosecond) time scale. Several residues in the loop that connects the β_1- and β_2-strands (T30–K38) also exhibit lower than average R_1 and NOE values.

R_2 values and R_2/R_1 ratios are elevated significantly above the average for residues T8, N12, S31, K37, and A51 and slightly above average for several other residues (Figures 2B and 2D). This effect may be indicative of slow (microsecond–millisecond) time scale conformational rearrangement in the vicinity of these residues. Alternatively, higher than average transverse relaxation for specific ^{15}N nuclei could be a result of anisotropic tumbling of the protein. Nuclei for which the associated NH bond vector is aligned parallel to the long axis of the diffusion tensor of an anisotropically tumbling molecule reorient more slowly than those aligned perpendicular to the long axis. Thus, the former have increased low frequency spectral densities and increased transverse relaxation (Kroenke et al., 1998). Several methods have been proposed to distinguish between increases in transverse relaxation resulting from anisotropic tumbling and those resulting from true slow time scale conformational exchange (Akke and Palmer, 1996; Fushman and Cowburn, 1998; Kroenke et al., 1998; Vis et al., 1998). In the present study, we used the method of Fushman and Cowburn (1998) in which the ratio of transverse auto relaxation rate (R_2) to the transverse cross relaxation rate (η_{xy}) is compared across the protein. For residues without large amplitude fast internal motion, this ratio is expected to be approximately constant in the absence of slow conformational exchange but to be elevated for those residues affected by slow conformational exchange. Values of η_{xy} and R_2/η_{xy} for each residue are shown in Figures 2E and 2F, respectively. Most residues in the core of the protein have R_2/η_{xy} values of ~1.7. However, all of the residues exhibiting high R_2/R_1 ratios (Figure 2D) also have high R_2/η_{xy} values (Figure 2F), indicating that the fast transverse relaxation of these residues is a result of true slow time scale conformational exchange. The high R_2/η_{xy} values for residues close to the N- and C-termini can likely be attributed to the presence of large amplitude fast internal motions as indicated by the negative NOE values for these residues (Figure 2C). However, slow time scale conformational exchange may also contribute to the high R_2/η_{xy} values for some of the residues near the N-terminus (see below).

Molecular rotational diffusion

The R_2/R_1 ratios for residues not subject to large amplitude fast internal motions or to slow time scale conformational exchange were used to estimate the components of the molecular rotational diffusion tensor. Calculations assuming a fully anisotropic diffusion tensor gave diffusion components (D_{zz}:D_{xx}:D_{yy}) in the ratio 1.40:1.29:1, indicating that the diffusion rate around the y-axis is significantly lower than those around the other two axes, but that diffusion rates around x- and z-axes differ by less than ~10%. Thus, these calculations suggested that the molecular rotational diffusion tensor may be approximated by an

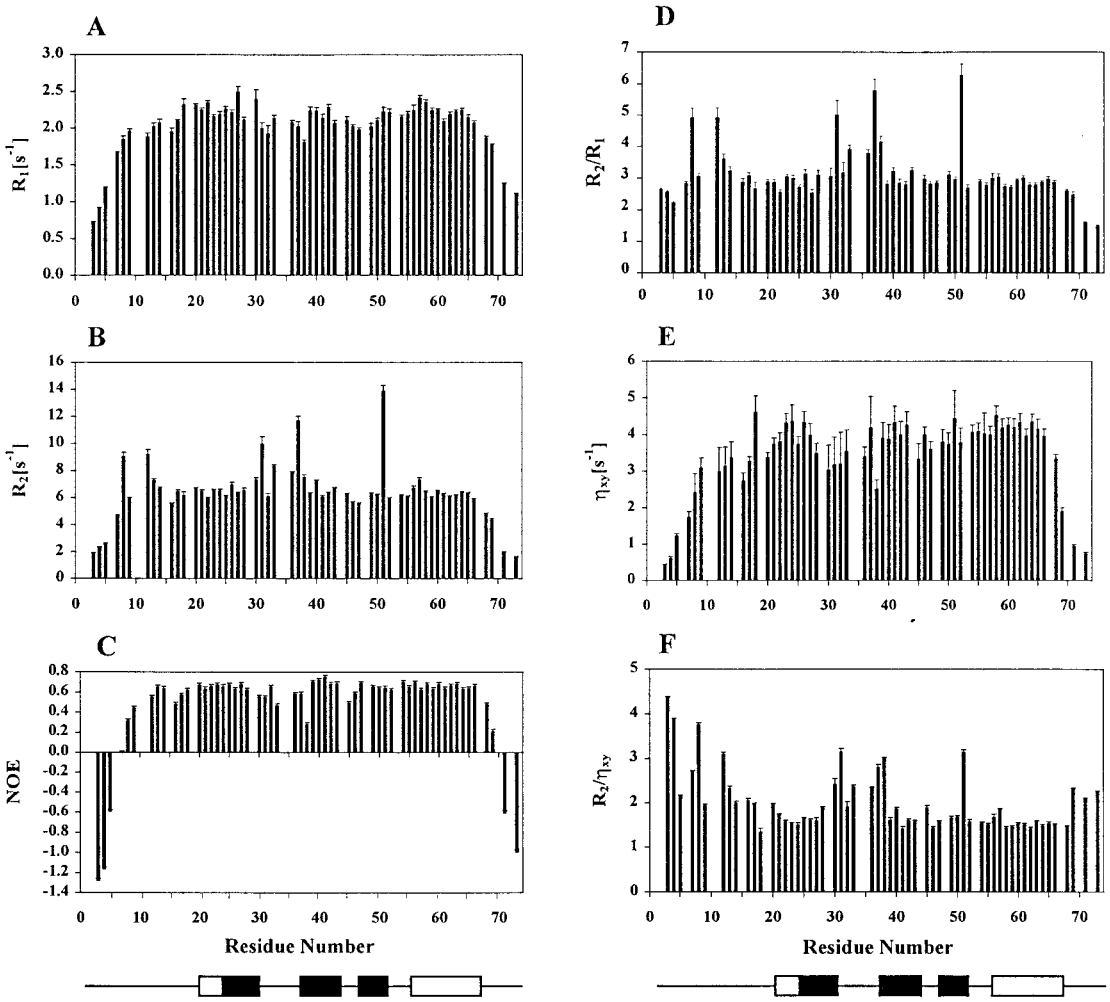

Figure 2. Plots of the relaxation parameters (A) R_1, (B) R_2, (C) $\{^1H\}$-^{15}N NOE, (D) R_2/R_1, (E) η_{xy}, and (F) R_2/η_{xy} as a function of residue number. The positions of the secondary structure elements of eotaxin are indicated at the bottom of each column as filled bars (β-strands) or open bars (turn of 3_{10}-helix or C-terminal α-helix).

oblate ellipsoid with $D_\parallel/D_\perp$ [$=2D_{yy}/(D_{xx}+D_{zz})$] = 0.74. Similarly, calculations assuming an axially symmetric diffusion tensor indicated that the data could be fitted to an oblate model with $D_\parallel/D_\perp = 0.82 \pm 0.04$ or a prolate model with $D_\parallel/D_\perp = 1.12 \pm 0.04$; this ambiguity has been discussed by Blackledge et al. (1998). The oblate model was selected as being most suitable for the current data set on the basis that: (1) it gave a slightly better fit than the prolate model to the experimental data ($\chi^2 = 90$ versus 99); (2) the fully anisotropic tensor calculations support the oblate model; (3) the improved agreement with the experimental data observed for the oblate axially symmetric model relative to the isotropic model is statistically significant ($p<0.05$) according to an F-statistic test ($F = 3.19$; Lee et al., 1997); and (4) the improved agreement with the experimental data observed for the fully anisotropic model relative to the oblate axially symmetric model is not statistically significant ($F = 0.87$; $p > 0.05$).

After selection of appropriate internal dynamics models and final model free calculations, the optimized effective molecular rotational correlation time τ_m was 5.09 ± 0.02 ns with $D_\parallel/D_\perp = 0.81 \pm 0.02$ and the unique (short) axis of the diffusion tensor oriented as indicated in Figure 4. Five of the NH vectors studied are aligned within 30° of the unique axis, 31 form angles of 30–60° with the unique axis, and the remaining 21 (including most of those in the β-sheet) form angles of 60–90° with the unique axis. Calcula-

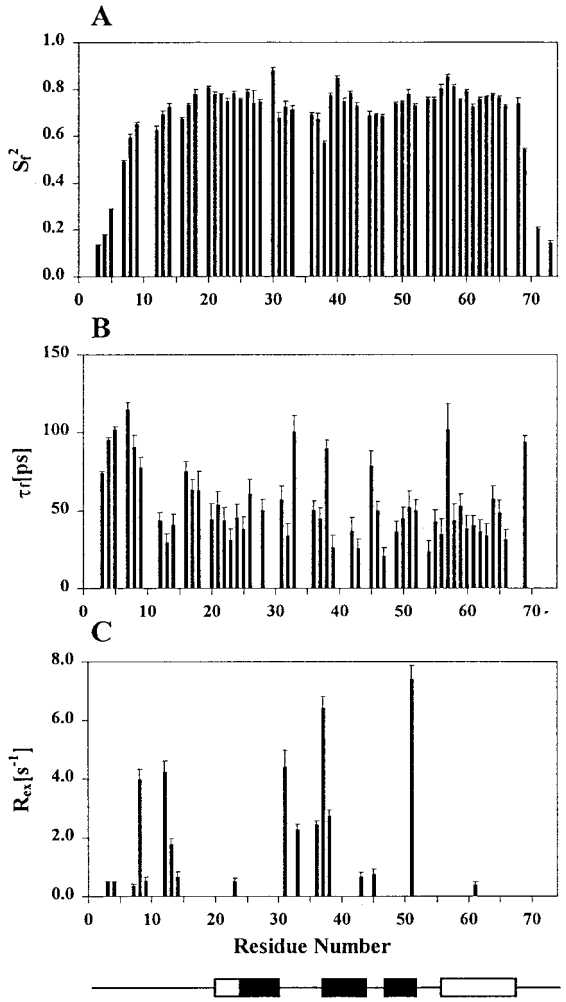

Figure 3. Plots of the model-free dynamics parameters (A) S_f^2, (B) τ_f and (C) R_{ex} as a function of residue number. The positions of the secondary structure elements of eotaxin are indicated at the bottom of each column as in Figure 2. The τ_f value of T30 is poorly defined (324 ± 290 ps) and is not shown in the figure. Slow time scale order parameters (not shown in the figure) were required for R27, K68, T71 and K73. S_s^2 values obtained for these residues were 0.88 ± 0.02, 0.73 ± 0.01, 0.62 ± 0.01 and 0.60 ± 0.01 respectively, and corresponding τ_s values were 3184 ± 820, 1045 ± 131, 811 ± 17 and 686 ± 16 ps, respectively.

tions assuming an isotropic rotational diffusion tensor gave a τ_m value of 5.20 ± 0.02 ns, similar to the effective τ_m for the axially symmetric diffusion model. Since the molecular weight of eotaxin is ∼8.4 kDa, a correlation time of ∼5 ns indicates that the protein exists predominantly as a monomer under the conditions of the NMR study. Crump et al. (1998) have determined the K_d for dimerization to be 8.5 mM at pH 5.0, 30 °C, and low salt conditions, consistent with the present results. Although the results presented here are for an axially symmetric diffusion tensor, it is noteworthy that analysis of the data using the isotropic model yielded internal motional parameters that were not significantly different from those obtained with the anisotropic model; results for both models are included in the Supplementary material.

Internal dynamics parameters

Internal motional parameters were obtained using the models described in Materials and methods. The data for 2 and 33 residues were adequately accounted for by Models 1 and 2, respectively. Data for 18 residues required incorporation of the exchange broadening term, R_{ex}; all of these were fit to Model 4. Finally, data for 4 residues could only be adequately described by Model 5, incorporating two time scales of internal motion faster than the τ_m. The sufficiencies of the fits were evaluated by comparison of the weighted sum of the squared residuals (SSE) to the 95% critical value (Stone et al., 1993; Mandel et al., 1995). According to this criterion, data for 45 residues (79%) were adequately fit at the 95% confidence level; residues not satisfying this criterion were K17, R22, S25, Y26, R28, T30, G32, I40, I49, D52, W57, and Q59. By comparison, data for 42 residues were adequately fit at the 95% confidence level in calculations assuming an isotropic rotational diffusion tensor.

The internal dynamics parameters optimized for each residue are plotted in Figure 3. The average generalized order parameter of backbone NH groups in eotaxin is 0.68 (standard deviation 0.18), which is substantially lower than the average order parameter of 0.84 ± 0.11 for the 20 proteins in the Indiana Dynamics Database (J.L. Goodman, M.D. Pagel, and M.J. Stone, unpublished results). Figure 4A shows the backbone structure of eotaxin, color coded according to the values of the fast time scale order parameters. The S_f^2 values range from 0.14 to 0.88 and appear to be dependent on secondary structural environment. In general, residues in the termini and in loops and turns are significantly more flexible than those in the three β-strands, the α-helix, and the single turn of 3_{10}-helix. Thus, the low average order parameter partly reflects the high proportion of residues in these flexible regions. The average order parameter for residues in secondary structure elements (0.75 ± 0.07) remains lower than the typical average for other proteins but is similar to the average values observed previously for the glucose permease IIA domain (Stone et al., 1992) and dihydrofolate re-

ductase (Epstein et al., 1995). Substantial variations of average order parameters have been observed between proteins previously studied by NMR relaxation methods. The causes of these differences are not well established, but may reflect differences in data collection and analysis methods as well as true differences between the dynamics of proteins with different structural folds and stabilities. In this regard it is interesting to note that eotaxin undergoes very rapid hydrogen exchange with solvent, suggesting that it is relatively thermally unstable (Crump et al., 1998).

The R_{ex} terms, indicative of microsecond to millisecond time scale conformational exchange, are plotted in Figure 3C. All nine residues that require R_{ex} terms greater than 1 s^{-1} also have elevated R_2/η_{xy} values indicating that the R_{ex} terms reflect true conformational exchange rather than the effects of anisotropic molecular diffusion. Most of the residues requiring R_{ex} terms are located in regions of the amino acid sequence adjacent to the four conserved cysteine residues. In particular, T7, T8, C9, N12, L13, and A14 are close to the first two cysteine residues (C9 and C10), S31, K33, Q36, K37 and A38 in the β_1-β_2 loop are close to the third cysteine (C34), and A51 immediately follows the fourth cysteine (C50). Furthermore, the backbone NH groups of C10 and F11 are not observed in the HSQC spectrum of eotaxin, presumably due to a very high degree of conformational exchange broadening. In addition, peaks in the HNCACB, CBCA(CO)NH, and CCC-TOCSY-NNH spectra corresponding to residues 8, 9, 12, and 13 tended to be somewhat weaker than other peaks in these spectra, suggesting increased transverse relaxation rates for the carbon and/or nitrogen nuclei in these residues (data not shown). Figure 4B illustrates the spatial proximity of NH groups exhibiting conformational exchange broadening to the two conserved disulfide bonds (C9-C34 and C10-C50). These results suggest that the residues near to the disulfide bonds may be experiencing a concerted conformational rearrangement. It is noteworthy that the absence of an R_{ex} term for C50 does not necessarily indicate the absence of motion on the μs–ms time scale because the R_{ex} value is dependent on the chemical shift difference and relative populations of the exchanging species as well as the rate of exchange (Palmer et al., 1996 and references therein). Dynamics parameters were not determined for C34 due to spectral overlap.

Discussion and conclusions

Fast time scale motions

The distribution of residues in eotaxin with large amplitude motion on a subnanosecond time scale is similar to those observed previously for the dimeric CXC chemokine interleukin-8 (IL-8; Grasberger et al., 1993) and the monomeric CC-chemokine viral macrophage inflammatory protein-II (vMIP-II; Liwang et al., 1999). In particular, all three chemokines have very low order parameters for residues on the N-terminal side of the CXC or CC motif and for the last two or three residues in the C-terminal α-helix. In addition, the order parameters reported here correlate well with the rmsd values for the calculated ensemble of eotaxin structures (Crump et al., 1998) and also with the tertiary structural differences between the CC chemokines RANTES and MCP-1 (Skelton et al., 1995; Handel and Domaille, 1996; Crump et al., 1998), suggesting that the variations in these structures may be attributed to true conformational flexibility rather than to lack of geometrical constraints in the disordered regions.

The N-terminus of chemokines has been identified as the most important region involved in activation of chemokine receptors (Crump et al., 1997, 1998, and references therein). Therefore, the observation that large amplitude flexibility occurs near the N-terminus of several chemokines suggests that flexibility of this region may be important for the mechanism of receptor activation. According to the two-step model (Murphy, 1994; Crump et al., 1997, 1998), the first step of receptor activation involves binding of the chemokine N-loop to the receptor, whereas the second step comprises two theoretically separable events – binding of the N-terminus to the receptor and a conformational change of the receptor. If the N-terminal region of the chemokine were rigid, then it is likely that the two events comprising step two would occur in a concerted manner, i.e. the conformational rearrangement of the receptor would bring it into contact with the static chemokine. On the other hand, if the bound chemokine were flexible then the N-terminus may come into contact with the receptor *before* the conformation of the receptor has changed significantly; this contact would then be *followed* by a conformational change of the receptor (and possibly the chemokine) causing the activation of the receptor. The current dynamics data, along with the previous data for IL-8 and vMIP-II (Grasberger et al., 1993; Liwang et al., 1999), indicate that indeed the N-terminus and the N-

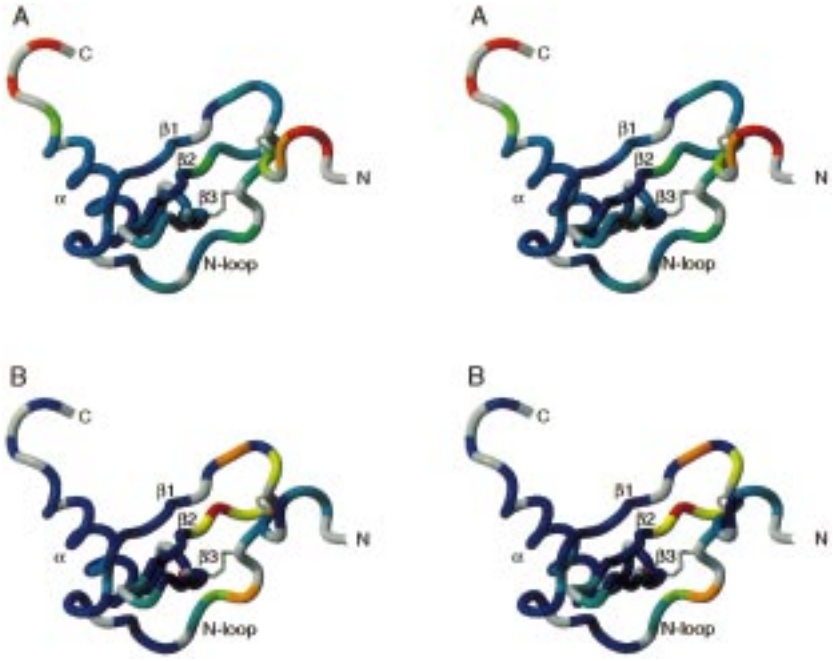

Figure 4. Stereoviews of the backbone C_α traces of eotaxin color coded according to the values of (A) the order parameters (S_f^2) and (B) the conformational exchange terms (R_{ex}). The unique axis of the diffusion tensor is aligned perpendicular to the plane of the page. Residues are colored in a continuous spectrum from red to blue, with red corresponding to the most flexible and blue to the most rigid regions. The color scale is: (A) red ($S_f^2 \leq 0.2$), yellow ($S_f^2 = 0.40$), green ($S_f^2 = 0.60$), and blue ($S_f^2 \geq 0.80$); and (B) red ($R_{ex} \geq 5\ s^{-1}$), yellow ($R_{ex} = 3\ s^{-1}$), green ($R_{ex} = 1\ s^{-1}$), and blue ($R_{ex} = 0\ s^{-1}$). Those residues whose relaxation data were not available due to spectral overlap are colored in gray. The side chains of the four conserved cysteine residues and the two disulfide bonds are shown as gray cylinders. Atomic coordinates were taken from the energy-minimized average NMR structure (PDB code 1EOT; Crump et al., 1998). This figure was prepared using the program MOLMOL (Koradi et al., 1996).

loop are both flexible and can undergo considerable motion relative to each other. Thus, these data are consistent with a mechanism in which the second binding event and the receptor conformational change occur sequentially.

Slow time scale conformational exchange

The ^{15}N exchange broadening terms calculated for eotaxin indicate that the residues adjacent to the two conserved disulfide bonds may be experiencing a concerted conformational rearrangement (Figure 4B). This conclusion is supported by the observation of defined local structure but apparent segmental motion and low backbone angular order parameters of the β_1–β_2 loop in the ensemble of NMR structures of eotaxin (Crump et al., 1998). A possible source of the observed slow conformational exchange may be isomerization of one or both disulfide bonds between the two most favored conformations. Typically, the dihedral angle around disulfide bonds (χ_3) is $\pm 90°$ (Creighton, 1993) and exchange between the two conformations is limited by an activation barrier of $\sim$7–9 kcal mol^{-1} (Fraser et al., 1971). Exchange kinetics on the μs–ms time scale, as observed in the present study, would require an activation barrier of $\sim$8–12 kcal mol^{-1}, similar to that expected for disulfide isomerization. Thus, it would not be surprising to observe conformational exchange broadening for nuclei adjacent to disulfide bonds. Indeed, NMR studies have revealed evidence of slow conformational exchange in the vicinity of disulfide bonds in basic pancreatic trypsin inhibitor (BPTI) (Szyperski et al., 1993; Beeser et al., 1997, 1998), the C-terminal Kunitz domain of human α3-chain type VI collagen (Sørensen et al., 1997), human type-α transforming growth factor (Li and Montelione, 1995), toxin α from *Naja nigricollis* (Guenneugues et al., 1997), and the denatured state of hen lysozyme (Schwalbe et al., 1997). In the solution structure of eotaxin (Crump et al., 1998) the C9-C34 disulfide bond is relatively poorly defined. Furthermore, it appears that this disulfide bond could undergo isomerization without any significant reorganization of the well-ordered regions

of the structure. Therefore it seems reasonable to propose disulfide bond isomerization as the source of the slow conformational exchange observed in the present study.

It is instructive to compare the slow conformational exchange behavior of eotaxin with that observed for other chemokines. The dimeric CXC-chemokine IL-8 displayed quite different exchange behavior from eotaxin, with R_{ex} terms prevalent in the α-helix and in β-sheet regions contacting the helix (Grasberger et al., 1993). These effects were interpreted as suggesting that the helix-sheet interface is dynamic on a μs–ms time scale. In contrast, the exchange behavior of the CC-chemokine vMIP-II (Liwang et al., 1999) was similar to that of eotaxin, with exchange terms required in the regions of the sequence surrounding the four conserved cysteine residues; exchange terms were also found in the 3_{10}-turn that precedes the β_1-strand. Both of these previous studies were performed assuming isotropic molecular tumbling, so it is possible that some of the R_{ex} terms observed reflect alignment of the relevant NH bond vectors along the long axis of the molecule. However, given that the cross-relaxation experiments for eotaxin confirmed that the R_{ex} terms arise from true conformational exchange, it seems likely that the R_{ex} terms found in the corresponding region of vMIP-II also reflect real conformational flexibility. Thus, it is possible that conformational exchange in the vicinity of the disulfide bonds is a common feature of CC-chemokines. The CC or CXC motif of chemokines is located between the N-terminus and the N-loop, the two regions implicated in receptor binding and activation. Therefore, conformational changes in this region could potentially allow for reorientation of these two regions relative to each other during receptor activation. Dynamics studies of additional chemokines will be required to determine whether disulfide bond flexibility is a general feature of CC-chemokines.

In summary, we have identified the regions of eotaxin that are conformationally mobile on subnanosecond and microsecond–millisecond time scales. Fast time scale flexibility of the N-terminal region appears to be a conserved feature of all chemokines and may be important in allowing this region to adopt a suitable conformation for activation of chemokine receptors. Flexibility on the slower time scale is limited to the immediate vicinity of the two conserved disulfide bonds, reflecting possible disulfide bond isomerization. A similar observation for vMIP-II (Liwang et al., 1999) suggests that this type of mobility may also be conserved among the CC-chemokines.

Acknowledgements

We gratefully thank Dr. Arthur G. Palmer III (Columbia University) for providing the Modelfree software package, Dr. Lewis Kay (University of Toronto) and Dr. Mark Rance (University of Cincinnatti) for providing pulse programs, and Michael Seewald for helpful discussions and for computer scripts. We also thank Drs. Mark D. Pagel and Ulrike Werner-Zwanziger of the Indiana University NMR facility for technical support. This work was supported by grants from the National Institutes of Health (GM-55055 to M.J.S.) and the National Science Foundation (MCB-9600968 to M.J.S.), and by an Established Investigator Award from the American Heart Association National Affiliate (to M.J.S.). Acknowledgement is made to the donors of The Petroleum Research Fund, administered by the American Chemical Society, for partial support of this research (to M.J.S.). This work was also supported by a predoctoral fellowship from the American Heart Association, Midwest Affiliate (to J.Y.).

References

Akke, M. and Palmer III, A.G. (1996) *J. Am. Chem. Soc.*, **118**, 911–912.

Baggiolini, M. (1996) *J. Clin. Invest.*, **97**, 587.

Baggiolini, M., Dewald, B. and Moser, B. (1997) *Annu. Rev. Immunol.*, **15**, 675–705.

Barbato, G., Ikura, M., Kay, L.E., Pastor, R.W. and Bax, A. (1992) *Biochemistry*, **31**, 5269–5278.

Bazan, J.F., Bacon, K.B., Hardiman, G., Wang, W., Soo, K., Rossi, D., Greaves, D.R., Zlotnik, A. and Schall, T.J. (1997) *Nature*, **385**, 640–644.

Beeser, S.A., Goldenberg, D.P. and Oas, T.G. (1997) *J. Mol. Biol.*, **269**, 154–164.

Beeser, S.A., Oas, T.G. and Goldenberg, D.P. (1998) *J. Mol. Biol.*, **284**, 1581–1596.

Blackledge, M., Cordier, F., Dosset, P. and Marion, D. (1998) *J. Am. Chem. Soc.*, **120**, 4538–4539.

Clore, G.M., Driscoll, P.C., Wingfield, P.T. and Gronenborn, A.M. (1990a) *Biochemistry*, **29**, 7387–7401.

Clore, G.M., Szabo, A., Bax, A., Kay, L.E., Driscoll, P.C. and Gronenborn, A.M. (1990b) *J. Am. Chem. Soc.*, **112**, 4989–4991.

Creighton, T.E. (Ed.) (1993) *Proteins: Structures and Molecular Properties*, W.H. Freeman and Company, New York, NY, pp. 18–19.

Crump, M.P., Gong, J.H., Loetscher, P., Rajarathnam, K., Amara, A., Arenzana-Seisdedos, F., Virelizier, J.L., Baggiolini, M., Sykes, B.D. and Clark-Lewis, I. (1997) *EMBO J.*, **16**, 6996–7007.

Crump, M.P., Rajarathnam, K., Kim, K.S., Clark-Lewis, I. and Sykes, B.D. (1998) *J. Biol. Chem.*, **273**, 22471–22479.
Epstein, D.M., Benkovic, S.J. and Wright, P.E. (1995) *Biochemistry*, **34**, 11037–11048.
Farrow, N.A., Muhandiram, R., Singer, A.U., Pascal, S.M., Kay, C.M., Gish, G., Shoelson, S.E., Pawson, T., Forman-Kay, J.D. and Kay, L.E. (1994) *Biochemistry*, **33**, 5984–6003.
Fraser, R.R., Boussard, G. and Saunders, J.K. (1971) *J. Am. Chem. Soc.*, **93**, 3822–3823.
Fushman, D. and Cowburn, D. (1998) *J. Am. Chem. Soc.*, **120**, 7109–7110.
Garcia-Zepeda, E.A., Rothenberg, M.E., Ownbey, R.T., Celestin, J., Leder, P. and Luster, A.D. (1997) *Nature Med.*, **2**, 449–456.
Grasberger, B.L., Gronenborn, A.M. and Clore, G.M. (1993) *J. Mol. Biol.*, **230**, 364–372.
Guenneugues, M., Drevet, P., Pinkasfeld, S., Gilquin, B., Menez, A. and Zinn-Justin, S. (1997) *Biochemistry*, **36**, 16097–16108.
Handel, T.M. and Domaille, P.J. (1996) *Biochemistry*, **35**, 6569–6584.
Kay, L.E., Torchia, D.A. and Bax, A. (1989) *Biochemistry*, **28**, 8972–8979.
Kelner, G.S., Kennedy, J., Bacon, K.B., Kleyensteuber, S., Largaespada, D.A., Jenkins, N.A., Copeland, N.G., Bazan, J.F., Moore, K.W., Schall, T.J. and Zlotnik, A. (1994) *Science*, **266**, 1395–1399.
Kitaura, M., Nakajima, T., Imai, T., Harada, S., Combadiere, C., Tiffany, H.L., Murphy, P.M. and Yoshie, O. (1996) *J. Biol. Chem.*, **271**, 7725–7730.
Koradi, R., Billeter, M. and Wüthrich, K. (1996) *J. Mol. Graph.*, **14**, 51–55.
Kroenke, C.D., Loria, J.P., Lee, L.K., Rance, M. and Palmer, A.G. (1998) *J. Am. Chem. Soc.*, **120**, 7905–7915.
Lee, L.K., Rance, M., Chazin, W.J. and Palmer III, A.G. (1997) *J. Biomol. NMR*, **9**, 287–298.
Li, Y.C. and Montelione, G.T. (1995) *Biochemistry*, **34**, 2408–2423.
Lipari, G. and Szabo, A. (1982a) *J. Am. Chem. Soc.*, **104**, 4546–4559.
Lipari, G. and Szabo, A. (1982b) *J. Am. Chem. Soc.*, **104**, 4559–4570.
Liwang, A.C., Cao, J.J., Zheng, H., Lu, Z., Peiper, S.C. and Liwang, P.J. (1999) *Biochemistry*, **38**, 442–453.
Luster, A.D. (1998) *New Engl. J. Med.*, **338**, 436–445.
Mandel, A.M., Akke, M. and Palmer III, A.G. (1995) *J. Mol. Biol.*, **246**, 144–163.
Mandel, A.M., Akke, M. and Palmer III, A.G. (1996) *Biochemistry*, **35**, 16009–16023.
Murphy, P.M. (1994) *Annu. Rev. Immunol.*, **12**, 593–633.
Palmer, A.G., Williams, J. and McDermott, A. (1996) *J. Phys. Chem.*, **100**, 13293–13310.
Palmer III, A.G., Rance, M. and Wright, P.E. (1991) *J. Am. Chem. Soc.*, **113**, 4371–4380.
Rothenberg, M.E., Luster, A.D., Lilly, C.M., Drazen, J.M. and Leder, P. (1995) *J. Exp. Med.*, **181**, 1211–1216.
Schwalbe, H., Fiebig, K.M., Buck, M., Jones, J.A., Grimshaw, S.B., Spencer, A., Glaser, S.J., Smith, L.J. and Dobson, C.M. (1997) *Biochemistry*, **36**, 8977–8991.
Skelton, N.J., Aspiras, F., Ogez, J. and Schall, T.J. (1995) *Biochemistry*, **34**, 5329–5342.
Sørensen, M.D., Bjøn, S., Norris, K., Olsen, O., Petersen, L., James, T.L. and Led, J.J. (1997) *Biochemistry*, **36**, 10439–10450.
Stone, M.J., Fairbrother, W.J., Palmer III, A.G., Reizer, J., Saier Jr., M.H. and Wright, P.E. (1992) *Biochemistry*, **31**, 4394–4406.
Stone, M.J., Chandrasekhar, K., Holmgren, A., Wright, P.E. and Dyson, H.J. (1993) *Biochemistry*, **32**, 426–435.
Szyperski, T., Luginbühl, P., Otting, G., Güntert, P. and Wüthrich, K. (1993) *J. Biomol. NMR*, **3**, 151–164.
Tjandra, N., Feller, S.E., Pastor, R.W. and Bax, A. (1995) *J. Am. Chem. Soc.*, **117**, 12562–12566.
Tjandra, N., Szabo, A. and Bax, A. (1996) *J. Am. Chem. Soc.*, **118**, 6986–6991.
Vis, H., Vorgias, C.E., Wilson, K.S., Kaptein, R. and Boelens, R. (1998) *J. Biomol. NMR*, **11**, 265–277.
Weller, P.F. (1994) *Curr. Opin. Immunol.*, **6**, 85–90.